J. Synchrotron Rad. (1998). **5**, 1085–1087

A bent Laue analyser crystal for Rayleigh-to-Compton computed tomography

Clemens Schulze[a]* and Ulf Kleuker[b]

[a]Swiss Light Source, PSI, CH-5232 Villigen PSI, Switzerland, and [b]European Synchrotron Radiation Facility, BP 220, F-38043 Grenoble CEDEX, France. E-mail: schulze@psi.ch

(*Received 4 August 1997; accepted 18 November 1997*)

A new optical system to perform tomography based on the Rayleigh-to-Compton (RC) method with high spatial and spectral resolution is presented. The RC technique allows the effective atomic number of a sample to be measured and finds application in bone mineral densitometry in medicine. It is particularly useful for the characterization of the distribution of biological materials which do not exhibit distinctive diffraction peaks. The system is based on the separation of the elastic line from the spectrum that is scattered by the sample by means of a bent Laue analyser crystal, and the subsequent independent detection of the elastic and inelastic parts of the spectrum with two large-area scintillation counters. The high energy resolution permits operation at low momentum transfer, where the RC method has its best contrast-to-noise ratio for low-Z materials. The geometrical and spectral requirements in terms of the incident beam and the conical analyser crystal are discussed. A first-generation tomographic imaging system (pencil beam, scanned sample) as implemented at the ESRF Compton-Scattering Station ID15B is described. A high-resolution tomographic reconstruction of a bone sample is presented.

Keywords: Rayleigh-to-Compton method; computed tomography; conical bending.

1. Introduction

The non-destructive detection of low- and medium-Z elements in bulk materials is cumbersome because their characteristic X-ray fluorescence lines are absorbed within the sample. The Rayleigh-to-Compton (RC) ratio method offers the capability to determine the mean atomic number of the probed volume by normalizing the intensity of the coherently scattered fraction of the spectrum to the intensity of the Compton scattered fraction (Puumalainen *et al.*, 1976). The RC technique does not provide atomic sensitivity, but, other than absorption tomography, it allows changes in composition to be distinguished from changes in density.

Due to the functionality of the basic differential cross sections, the sensitivity of the RC method to the effective atomic number increases with scattering angle, while the precision decreases owing to poorer counting statistics. Recently, Harding *et al.* (1995) demonstrated that for low-Z materials the best contrast-to-noise ratio is found in forward-scattering geometry (low momentum transfer). In the best q-regime of about 0.5 Å^{-1}, the Compton shift is of the order of 100 eV or 2×10^{-3} and cannot be resolved by conventional solid-state detectors. Stimulated by these findings, we developed a new approach to the RC technique involving: (i) atomic-number-optimized RC with a scattering-angle tunable device; (ii) tomographic imaging employing reconstruction algorithms. The angular tunability allows the contrast to be optimized for samples of different mean atomic number, since the optimal momentum transfer depends on ΔZ of the probed volume elements. The tomographic reconstruction approach eliminates mapping errors which can arise in point-scanning techniques in forward and backscattering geometry from overlapping volume elements.

This paper addresses the geometrical and spectral requirements imposed by the imaging technique. A simple bending device for conical crystal bending and its performance are presented and tomographic results are shown. The theoretical background related to the tomographical RC approach and an evaluation of the contrast-to-noise ratio was recently published elsewhere (Kleuker & Schulze, 1997).

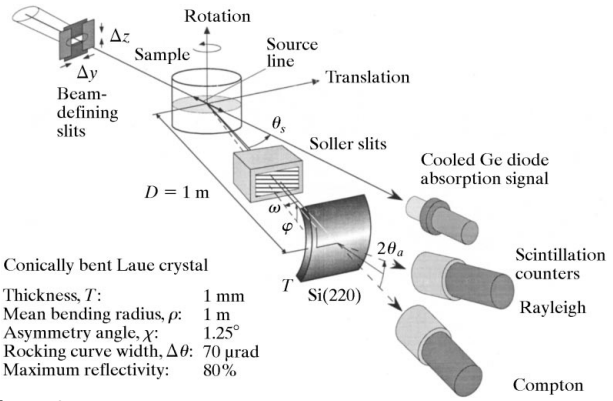

Figure 1
Scheme of the set-up for wavelength-dispersive RC computed tomography. The incident beam is monochromated and focused by means of an Si(331) Bragg monochromator in Johann geometry delivering 6×10^{11} photons s^{-1} vertically integrated in a focal line of 350 μm. The bandwidth is 4×10^{-4} at 60 keV.

2. Experimental set-up

Our approach to Rayleigh-to-Compton-based computed tomography (RC-CT) is based on the use of a bent analyser crystal. A bent Laue crystal in inverse Cauchois geometry (Cauchois, 1932) provides an energy resolution better than 10^{-3}, sufficient to separate the elastic signal from the inelastic one at low momentum transfer. Fig. 1 shows the experimental set-up. A focused and collimated beam probes the sample and is subsequently recorded by a cooled Ge diode. The scattered spectrum is observed under a mean horizontal scattering angle, θ_s, and a solid angle defined by the Soller slits. The analyser crystal is set to the energy of the elastic line so that the coherently and incoherently scattered fraction of the beam can be detected separately after a short distance by two scintillation counters.

2.1. *Requirements on primary beam and analyser crystal*

Analysis of the contrast-to-noise ratio as a function of the efficiency of the Laue crystal analyser reveals that the average reflectivity must exceed 25% in order to provide a contrast-to-noise ratio superior to that achievable with solid-state detectors (Kleuker & Schulze, 1997). This imposes stringent requirements on the primary beam as well as on the analyser crystal. Assuming Gaussian distributions of all contributing components, the relation between the total angular width of the primary beam and the rocking curve width of the analyser, $\Delta\theta$, can be

expressed as

$$[(\Delta z/D)^2 + (\Delta E \tan\theta_a/E)^2 + (\varphi_{\max}\,\Delta y/D\sin\theta_s)^2]^{1/2} \leq \Delta\theta, \quad (1)$$

where Δz denotes the height of the primary beam, $\Delta E/E$ its bandwidth and Δy its breadth, D is the distance between the sample and analyser, θ_a and θ_s are the Bragg angle of the analyser crystal and the mean horizontal sample scattering angle, respectively, and $\varphi_{\max}$ is the maximal vertical scattering angle accepted by the analyser.

The rocking curve width of bent Laue crystals can be conveniently tailored by the intermediacy of the crystal asymmetrical angle. However, after passing through a maximum close to unity, the maximal reflectivity starts to decrease when the asymmetry angle is further increased due to the creation of new wave fields (Balibar *et al.*, 1983). This imposes an upper limit on the rocking curve width which is proportional to the structure factor of the reflection. For practical reasons the Si(220) reflection was chosen, which provides a maximal reflectivity of 0.8 at an asymmetry angle, χ, of 1.25° for the conditions presented in Fig. 1 (Schulze & Chapman, 1995).

2.2. *Aberrations*

A focused beam probing an extended sample as shown in Fig. 1 presents a line source rather than a point source. Along this line source the distance between the point sources and analyser crystal changes. Hence, the bending radius $\rho = D/\cos(\chi + \theta_a)$ has to vary linearly along the cylinder axis in order to realize the inverse Cauchois condition for all points of the line source. However, photons which are scattered under a horizontal angle, ω, different from 0° meet a bending radius which does not correspond to its distance from the crystal. This difference in bending radius is equivalent to an angular error. Fig. 2 shows the angular deviation from the monochromatic Bragg angle setting of the analyser crystal as a function of the horizontal and vertical scattering angle for a point source. Spherical aberrations as well as the energy shift due to the horizontal scattering angle ($\lambda' = \lambda\cos\omega$) are also taken into account. Note that the total angular error has positive as well as negative sign giving rise to signal mixing, which would prevent a quantitative analysis of the RC ratio. However, since the angular error in the vicinity of ω = 0° is much smaller than the rocking curve width of 70 µrad, vertical Soller slits can be used to confine the scattered photons to this angular range, thereby suppressing the signal mixing efficiently.

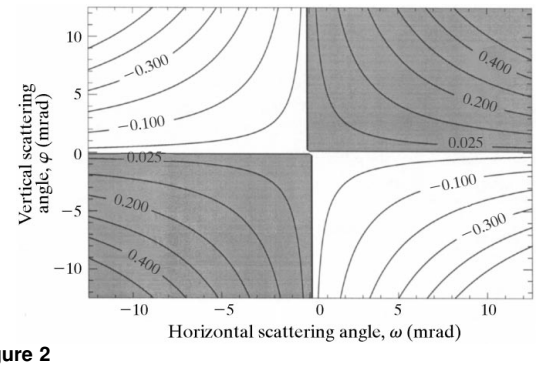

Figure 2
Total angular deviation from exact Bragg angle setting of the analyser crystal in units of mrad as a function of the horizontal and vertical opening angle for conical bending for the same experimental parameters as given in Fig. 1.

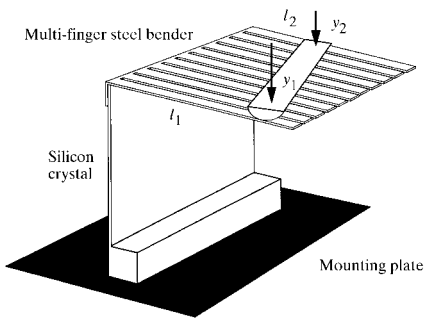

Figure 3
Bending mechanism of multi-finger bender for conical crystal bending.

2.3. *Conical bending*

Conical bending can be achieved using a four-point bender by varying the bending moment along the crystal plate. Since four-point benders are technically demanding, we designed a simple crystal bender based on the principle of the moment bender.

For an elastic straight beam with one end fixed and the other free, the inverse bending radius, $1/\rho$, is proportional to the applied moment, M,

$$\rho = (EI)_{\rm crystal}/M = l^2(EI)_{\rm crystal}/y_a\,3(EI)_{\rm spring}, \quad (2)$$

where E is the modulus of elasticity, I is the moment of inertia, l is the length of the spring, and y_a is its displacement at the position l (Roark & Young, 1985). When the ratio of l and y_a are chosen correctly, a linear variation of the spring length and the vertical displacement over the crystal width provides conical bending. Fig. 3 shows the principle of the multi-finger bender.

3. Experimental results

Experiments were performed at hutch B of ESRF's high-energy beamline ID15 (Suortti & Tschentscher, 1995). Experimental details are summarized in Fig. 1.

3.1. *Conical bending*

The local bending radius of the analyser crystal was determined by measuring the reflection angle of a monochromatic pencil beam while scanning the analyser crystal in the horizontal and the vertical directions. Fig. 4 displays the result for the central region of the analyser crystal for a vertical spring displacement between 4.5 and 12.0 mm and constant spring

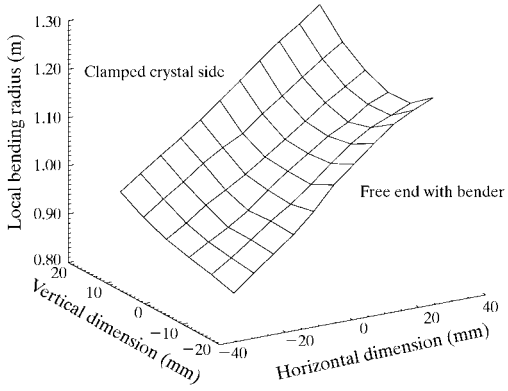

Figure 4
Measured local bending radius of the analyser crystal for a conical gradient corresponding to a scattering angle of 12°.

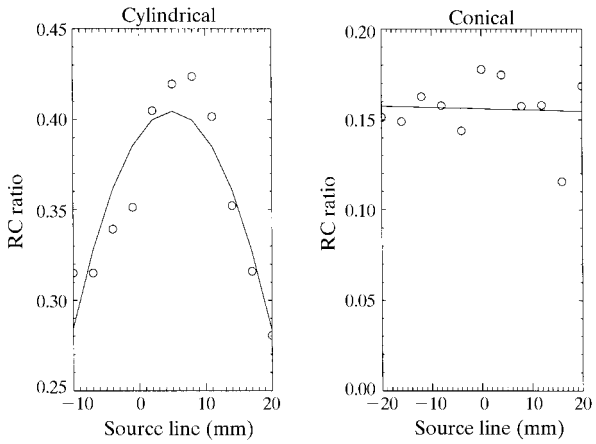

Figure 5
Comparison of depth of field aberration for (*a*) cylindrical and (*b*) conical analyser geometry. The acceptance of the Soller slit is 0.4° in both cases.

length. The gradient of the bending radius in the centre is satisfactory and the small deviation is probably caused by the constant spring length. In the vertical direction the bending radius is not constant. This might be due to a buckling of the crystal plate under the strong force applied to the springs. The effect could be eliminated by applying a bending moment at either side of the crystal so that the forces compensate.

3.2. *Depth of field*

The effect of the changing distances between source points and crystal was simulated by measuring the RC ratio of a glass capillary (Ø: 1 mm), filled with InGa-eutecticum, as a function of the source position along the primary beam. Fig. 5 shows the comparison of the RC contrast for cylindrical and conical bending of the analyser crystal. The same Soller slit of 0.4° was used in both measurements. Obviously conical bending compensates for the different distances between source point and analyser. However, due to the angular error presented by changing bending radii, the contrast is lower than in the cylindrical case.

3.3. *Reconstruction*

In order to test the feasibility of the tomographic approach to RC imaging, the trabecular structure of a vertebrae bone embedded in epoxy glue was tomographically scanned. The size of the probing beam was 100 µm horizontally and 50 µm vertically. The analyser was set to the maximum of the elastic line (θ_a = 3.08°) of the scattered spectrum and the sample was scanned with a step size of 100 µm (100 steps) and an angular increment of 2° (90 steps). The number of photons collected in the counters at each step was in excess of 10^4. Fig. 6 shows the reconstruction images of the transmitted, Compton and Rayleigh signal and also the RC ratio. The trabecular fine structure is clearly visible in all images. The images are free of artifacts due to elongated volume elements. Finally, the absorption effect visible in the Rayleigh and Compton images (pixels at the periphery have a higher count rate than those in the centre) are non-existent in the RC-ratio image.

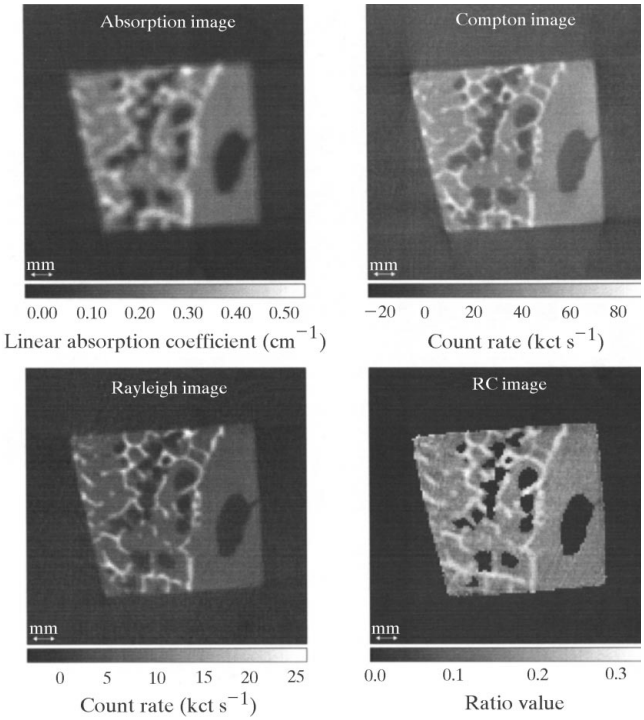

Figure 6
Series of reconstructed images of a vertebra bone imaged at a photon energy of 60 keV and a momentum transfer of 0.5 Å^{-1}

4. Conclusions and outlook

The proposed tomographical RC technique allows the distribution of low-Z elements in bulky samples to be measured at maximum contrast-to-noise ratio. Conical bending of the analyser crystal compensates distance errors. However, the bending has to be more homogeneous to reduce aberrations, thereby increasing counting statistics and RC ratio. This can be achieved either using a more elaborate bending technique or by the force-free application of the bending moments.

With a reliable calibration being available and an improved bending mechanism, Rayleigh-to-Compton computed tomography is feasible and offers a new approach to the two-dimensional quantification of low-Z materials.

The experiments were carried out at the ESRF high-energy beamline 15B under proposal numbers MI-183 and MI-220. We thank the beamline staff and in particular T. Buslaps for help during the experiments.

References

Balibar, F., Chukhovskii, F. N. & Malgrange, C. (1983). *Acta Cryst.* A**39**, 387–399.
Cauchois, Y. (1932). *J. Phys. Radium Ser. 7*, **3**, 320–336.
Harding, G., Armstrong, R., McDaid, S. & Cooper, M. (1995). *Med. Phys.* **22**(12), 2007–2014.
Kleuker, U. & Schulze, C. (1997). *Proc. SPIE*, **3149**, 177–185.
Puumalainen, P., Uimarihuhta, A., Alhva, E. & Olkkonen, H. (1976). *Radiology*, **120**, 723.
Roark, R. J. & Young, W. C. (1985). *Formulas for Stress and Strain.* Auckland: McGraw–Hill.
Schulze, C. & Chapman, D. (1995). *Rev. Sci. Instrum.* **66**(2), 2220–2223.
Suortti, P. & Tschentscher, T. (1995). *Rev. Sci. Instrum.* **66**(2), 1798–1801.